ChemComm

COMMUNICATION

Solid state precursor strategy for synthesizing hollow TiO$_2$ boxes with a high percentage of reactive {001} facets exposed†

Shuifen Xie, Xiguang Han, Qin Kuang,* Jie Fu, Lei Zhang, Zhaoxiong Xie* and Lansun Zheng

Three-dimensional, hollow, anatase TiO$_2$ boxes, each was enclosed by six single-crystalline TiO$_2$ plates exposed with highly reactive {001} facets, were facilely obtained by calcining a cubic TiOF$_2$ solid precursor at 500–600 °C. The formation of such particular nanostructures is attributed to the hard self-template restriction and the adsorption of F$^-$ ions from the TiOF$_2$.

Methodologies for morphologically tailored synthesis of metal and metal oxide nanomaterials have attracted remarkable attention, due to the intrinsic shape-dependent properties of nanocrystals.[1–5] As the most promising photocatalyst, anatase titanium dioxide (TiO$_2$) has been intensively investigated for the purpose of improving its photocatalytic performance. Early theoretical and experimental studies have shown that the high energy {001} facets of anatase TiO$_2$ in the equilibrium state are particularly reactive.[6] Unfortunately, most synthetic and naturally grown TiO$_2$ crystals are dominated by the thermodynamically stable and less chemically reactive {101} facets,[7–9] because the high energy facets generally grow fast and finally vanish to minimize the surface energy during crystal growth.[10] An important breakthrough was made by Lu *et al.*, who successfully synthesized TiO$_2$ single microcrystals with 47% {001} facets using F$^-$ as a morphology controlling agent.[11] Subsequently, our group increased the percentage of {001} facets to 89% by a hydrothermal route and demonstrated the extremely high photocatalytic reactivity of TiO$_2$ {001} facets in organic-dye degradation.[12] After that, many works have focused on the synthetic method of preparing TiO$_2$ nanocrystals exposed by {001} facets and the exploration of their applications in the utilization of solar energy.[13–16] However, most of these works are based on the surfactant-assisted hydrothermal method and only a few reports are concerned with other synthetic approaches. For example, an

electrospinning process was developed by Xia's group for preparing {001} facets-exposed TiO$_2$ nanocrystals.[17] However, the percentage of exposed {001} facets in the reported products is only 9.6%, which is still minor. Meanwhile, Ohtani and co-workers reported the preparation of anatase TiO$_2$ decahedra with 40% {001} facets by a gas-phase reaction route.[18] However, an extremely high temperature (1573 K) was required during the synthetic process. Hence, it is still a challenge to explore more facile methods for the fabrication of anatase TiO$_2$ photocatalysts with a high percentage of {001} facets. In this communication, we report the synthesis of anatase TiO$_2$ boxes with {001} facets by simply decomposing a TiOF$_2$ sub-micron cube precursor. Each of the as-prepared TiO$_2$ boxes consist of six single-crystalline nanoplates with a thickness of 40–50 nm, in which the {001} facets account for > 83% of all facets. Although the conversion from TiOF$_2$ to TiO$_2$ has been discovered before,[19,20] to the best of our knowledge this is the first case of preparing anatase TiO$_2$ exposed with a high-percentage of {001} facets *via* a solid phase route. The experimental data confirmed that these TiO$_2$ boxes exhibited a high performance in photocatalytic H$_2$ evolution.

Firstly, cubic TiOF$_2$ sub-micron crystals were successfully synthesized through a one-step solvent-thermal reaction using tetrabutyl titanate, hydrofluoric acid, and acetic acid (experimental details are given in the ESI†). Figs 1a and b show the as-prepared TiOF$_2$ precursors and clearly indicate that the TiOF$_2$ precursors are all well-defined sub-micron cubes with a uniform edge length of around 400–500 nm (the crystal phases were analyzed by X-ray diffraction as shown in Fig. S1, ESI†). TEM characterization further indicates that the TiOF$_2$ cubes are well-crystalized, with intrinsic {100} facets exposed (Fig. S2, ESI†). Then, TiOF$_2$ sub-micron cubes were calcined at different temperatures for 120 min. Figs 1c and d show the morphology of the products calcined at 500 °C (denoted as T500), indicating that the solid TiOF$_2$ sub-micron cubes have been converted into hollow TiO$_2$ boxes of equal size (the crystal phases are shown in Fig. S1, ESI†). Each of the hollow boxes is enclosed by six TiO$_2$ plates. It was found that the TiO$_2$ hollow boxes tend to be open and collapse into TiO$_2$ plates with a thickness of around 40–50 nm (according to the SEM image along the direction perpendicular to the thickness, Fig. S3, ESI†).

State Key Laboratory for Physical Chemistry of Solid Surfaces and Department of Chemistry, College of Chemistry and Chemical Engineering, Xiamen University, Xiamen, 361005, P.R. China. E-mail: zxxie@xmu.edu.cn, qkuang@xmu.edu.cn; Fax: +86-592-2183047; Tel: +86-592-2180627

† Electronic supplementary information (ESI) available: Experimental details, XRD patterns, TEM characterization of a single TiOF$_2$ cube, SEM image of the T500, TGA curve, SEM image of T300, UV-vis diffuse reflection spectra of the products obtained at different temperatures and the photocatalytic H$_2$ evolution activity comparison of T600 and P25. See DOI: 10.1039/c1cc11542a
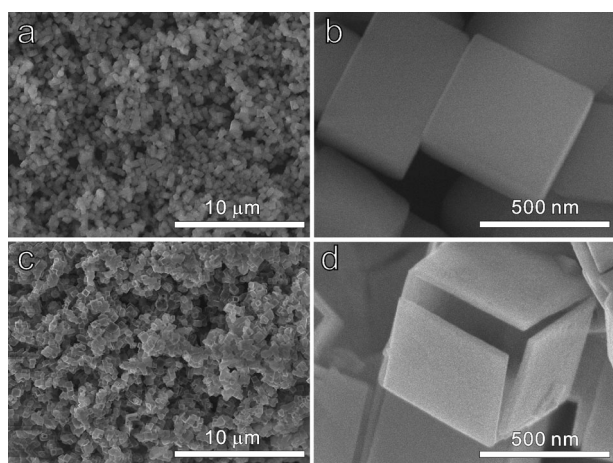
Fig. 1 (a) and (b) SEM images of the as-synthesized TiOF$_2$ sub-micron cubes, (c) and (d) SEM images of the hollow TiO$_2$ boxes (T500).

The TEM technique was adopted to further investigate the structure of the products. The hollow TiO$_2$ box-like structure of T500 can be clearly observed in Fig. 2a. In Fig. 2b, an individual TiO$_2$ nanoplate with a width of 400–500 nm was imaged, which corresponds well to the width found in the SEM image. The corresponding SAED pattern (Fig. 2e) can be indexed by the diffraction from the [001] zone axis, indicating that the top and bottom surfaces of the nanoplate are high energy {001} facets. The TEM image of an erect TiO$_2$ plate (Fig. 2d) shows that the angle between the side surface and the dominant bottom/top surface is about 112°, agreeing well with the angle between {001} and {101} facets. The lattice space of the side surface was measured to be 0.353 nm, corresponding to the thermodynamically stable {101} facets (Fig. 2e). Hence, these thin TiO$_2$ plates are enclosed by dominant {001} facets and minor {101} facets, as shown in the schematic illustration (Fig. 2f). The percentage of the reactive {001} facets can be estimated from the geometric calculation to be higher than 83% in this structure.
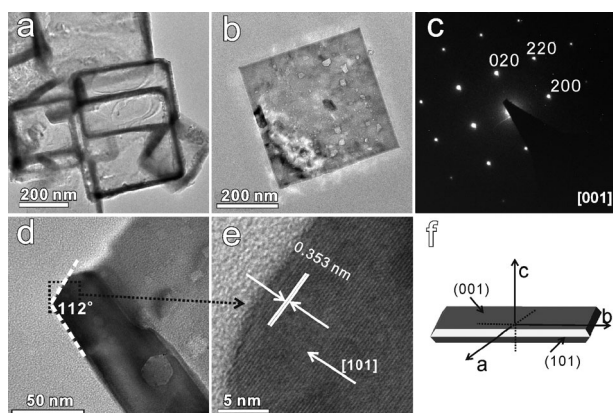
Fig. 2 (a) A TEM image of the hollow TiO$_2$ boxes (T500), (b) a TEM image of a single {001} plate from the hollow TiO$_2$ boxes after ultrasonic treatment and (c) the corresponding SAED pattern, (d) a TEM image of an erect TiO$_2$ plate, (e) a high-resolution TEM image recorded from the TiO$_2$ plate side surface marked with a dashed rectangle and (f) a schematic illustration showing the orientation of the TiO$_2$ plate.

To further understand the conversion process from TiOF$_2$ cubes to hollow TiO$_2$ boxes, the thermal stability of the as-synthesized TiOF$_2$ cubes was investigated. It was found that the decomposition of the TiOF$_2$ sample starts at around 300 °C, and this completely turns into TiO$_2$ when the temperature reaches 500 °C (see the thermogravimetric analysis (TGA) result shown in Fig. S4, ESI†). A sharp loss of weight and a distinct endothermic peak were found from 400 °C to 500 °C, indicating a rapid decomposition of TiOF$_2$. This thermal stability of TiOF$_2$ agrees with that reported previously.[19,20] The total weight loss of more than 50% is due to the following decomposition reaction: $2TiOF_2 = TiO_2 + TiF_4\uparrow$. From the XRD measurements (Fig. S1, ESI†), we found that both TiOF$_2$ and anatase TiO$_2$ existed when the calcination temperature is 300 °C (the T300 sample). With the increase in calcined temperature, the diffraction peaks corresponding to the TiOF$_2$ phase decreased and completely disappeared at 500 °C. This result is in agreement with the TGA analysis. It is remarkable that these anatase TiO$_2$ samples prepared by this precursor route are thermally stable up to 900 °C, which is much higher than the anatase-to-rutile transition point of 500 °C for hydrothermal samples.[21,22] We deduce that this may be attributable to the stabilization of surface adsorbed F$^-$ ions.

The SEM image (Fig. S5, ESI†) of T300 products apparently visualizes that the decomposition starts from the surface of the TiOF$_2$ cubes. Fig. 3 summarizes the phase conversion process from TiOF$_2$ cubes to hollow TiO$_2$ boxes. In the first decomposition stage, because of hard self-template restriction, the generated TiO$_2$ was shaped into plates. A similar role of TiOF$_2$ as hard templates was also found in a very recent study reported by Qiao and Yang et al.,[23] where TiOF$_2$ is a intermediate of the hydrothermal process to generate micro-sized TiO$_2$ nanosheets dominated by {001} and {100} facets. Further decomposition of TiOF$_2$ cubes results in the formation of the hollow box enclosed with six nanoplates. Meanwhile, we believe that the adsorption of F$^-$ ions on the surface must also be an essential factor for the formation of {001} facets-exposed TiO$_2$ plates, because a sufficient number of reports have confirmed the capability of F$^-$ ions for fabricating {001} facets-exposed anatase photocatalysts.[11–13]

Since this precursor strategy is a solid-state reaction, the crystallinity of the products, which is an important factor in
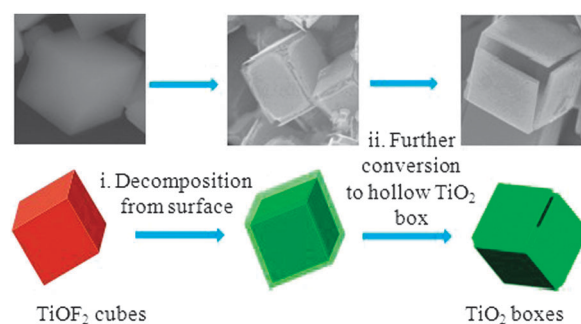
Fig. 3 A schematic of the procedure for preparing cubic TiO$_2$ boxes built by single-crystalline {001} facets-exposed plates from cubic TiOF$_2$ precursor.
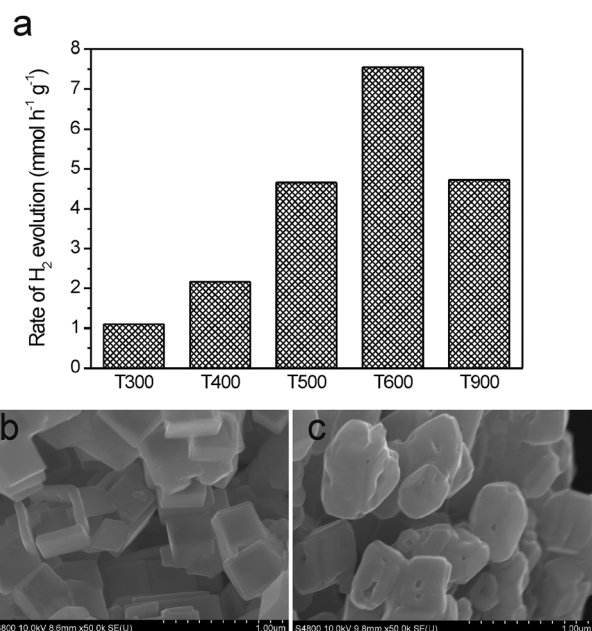
Fig. 4 (a) The photocatalytic H_2 evolution under UV-vis irradiation (220–770 nm) of the products calcined at various temperatures. (b) The SEM image of T600 and (c) the SEM image of T900.

photocatalysis,[24] can be facilely improved by increasing the calcining temperature. Usually, a higher temperature is beneficial for obtaining well-crystallized TiO_2 products with fewer crystal defects. To investigate the influence of crystallinity, the photocatalytic H_2 production rates catalyzed by the products gained at different temperatures were evaluated (experimental details, ESI†). In the experiments, 1 wt% Pt was loaded onto the TiO_2 photocatalysts as a co-catalyst and methanol was selected as a scavenger. Although the UV-vis diffuse reflection spectra (Fig. S6, ESI†) demonstrate that all of the products have the same light response in the UV region, their photocatalytic H_2 evolution capacities are quite different. As Fig. 4a shows, with a rise in the treatment temperature from 300 °C to 600 °C, the products exhibit increasing reactivity in photocatalytic H_2 evolution. Particularly, the T600 product presents the highest photocatalytic H_2 evolution rate of 7.55 mmol g^{-1} h^{-1}. This photocatalytic activity improvement can be attributed to two factors. Initially, the mass ratio of the {001} facets-exposed TiO_2 plates increases in the products from T300 to T500. Another reason is that, as the temperature increases, the generated TiO_2 plates have a higher degree of crystallinity, which favours elimination of crystal defects and greatly enhances the separation of photogenerated electrons and holes. However, when the calcining temperature is increased up to 900 °C, a large mass of the TiO_2 box-like products collapsed and this resulted in irregularly shaped TiO_2 structures (Fig. 4c), while the T600 samples (Fig. 4b) still sustained well-defined {001} facets-exposed plate structures. Thus, we now know that 900 °C is excessive for maintaining the {001} facet-exposed plate structures of TiO_2 in this case. Due to this change in morphology, the photocatalytic H_2 evolution rate of the T900 products decreases to a value of 4.72 mmol g^{-1} h^{-1} instead. Moreover, the surface area normalized photocatalytic H_2 evolution rate of T600 is even

higher than that of the commercially available photocatalyst Degussa P25 (Fig. S7, ESI†). All of these results further confirm that the {001} facets-exposed plate structures are beneficial for enhancing the photocatalytic activity of anatase TiO_2.

In summary, we developed a solid state precursor strategy for preparing box-like anatase TiO_2, using cubic $TiOF_2$ as precursor. Because of the hard self-template restriction and the adsorption of F^- ions, these cubic $TiOF_2$ can be facilely converted to hollow anatase TiO_2 boxes enclosed by six single-crystalline nanoplates with highly reactive {001} facets exposed. Due to the high percentage of reactive {001} facets, such novel TiO_2 boxes exhibit a good performance in photocatalytic H_2 evolution, which has been demonstrated to improve with an increase in the crystallinity of the products. We anticipate that this precursor strategy can have some implications for designing high activity TiO_2 photocatalysts and even other functional materials.

Notes and references

1 R. Narayanan and M. A. El-Sayed, *Nano Lett.*, 2004, **4**, 1343.
2 N. Tian, Z. Y. Zhou, S. G. Sun, Y. Ding and Z. L. Wang, *Science*, 2007, **316**, 732.
3 X. W. Xie, Y. Li, Z. Q. Liu, M. Haruta and W. J. Shen, *Nature*, 2009, **458**, 746.
4 Y. Y. Ma, Q. Kuang, Z. Y. Jiang, Z. X. Xie, R. B. Huang and L. S. Zheng, *Angew. Chem., Int. Ed.*, 2008, **47**, 8901.
5 J. A. Zhang, M. R. Langille, M. L. Personick, K. Zhang, S. Y. Li and C. A. Mirkin, *J. Am. Chem. Soc.*, 2010, **132**, 14012.
6 X. Q. Gong and A. Selloni, *J. Phys. Chem. B*, 2005, **109**, 19560.
7 B. H. Wu, C. Y. Guo, N. F. Zheng, Z. X. Xie and G. D. Stucky, *J. Am. Chem. Soc.*, 2008, **130**, 17563.
8 Y. W. Jun, M. F. Casula, J. H. Sim, S. Y. Kim, J. Cheon and A. P. Alivisatos, *J. Am. Chem. Soc.*, 2003, **125**, 15981.
9 U. Diebold, *Surf. Sci. Rep.*, 2003, **48**, 53.
10 D. Q. Zhang, G. S. Li, X. F. Yang and J. C. Yu, *Chem. Commun.*, 2009, 4381.
11 H. G. Yang, C. H. Sun, S. Z. Qiao, J. Zou, G. Liu, S. C. Smith, H. M. Cheng and G. Q. Lu, *Nature*, 2008, **453**, 638.
12 X. G. Han, Q. Kuang, M. S. Jin, Z. X. Xie and L. S. Zheng, *J. Am. Chem. Soc.*, 2009, **131**, 3152.
13 H. G. Yang, G. Liu, S. Z. Qiao, C. H. Sun, Y. G. Jin, S. C. Smith, J. Zou, H. M. Cheng and G. Q. Lu, *J. Am. Chem. Soc.*, 2009, **131**, 4078.
14 M. Liu, L. Y. Piao, L. Zhao, S. T. Ju, Z. J. Yan, T. He, C. L. Zhou and W. J. Wang, *Chem. Commun.*, 2010, **46**, 1664.
15 S. W. Liu, J. G. Yu and M. Jaroniec, *J. Am. Chem. Soc.*, 2010, **132**, 11914.
16 X. Y. Ma, Z. G. Chen, S. B. Hartono, H. B. Jiang, J. Zou, S. Z. Qiao and H. G. Yang, *Chem. Commun.*, 2010, **46**, 6608.
17 Y. Q. Dai, C. M. Cobley, J. Zeng, Y. M. Sun and Y. N. Xia, *Nano Lett.*, 2009, **9**, 2455.
18 F. Amano, O.-O. Prieto-Mahaney, Y. Terada, T. Yasumoto, T. Shibayama and B. Ohtani, *Chem. Mater.*, 2009, **21**, 2601.
19 N. M. Laptash, E. B. Merkulov and I. G. Maslennikova, *J. Therm. Anal. Calorim.*, 2000, **63**, 197.
20 J. C. Lytle, H. Yan, R. T. Turgeon and A. Stein, *Chem. Mater.*, 2004, **16**, 3829.
21 J. Ovenstone and K. Yanagisawa, *Chem. Mater.*, 1999, **11**, 2770.
22 S. Perera and E. G. Gillan, *Chem. Commun.*, 2005, 5988.
23 C. Z. Wen, J. Z. Zhou, H. B. Jiang, Q. H. Hu, S. Z. Qiao and H. G. Yang, *Chem. Commun.*, 2011, **47**, 4400.
24 A. Kudo and Y. Miseki, *Chem. Soc. Rev.*, 2009, **38**, 253.